Assessment of Broadband Shielding Effectiveness of Composite Panels for Protective Enclosures

Paul Clerico, Lionel Pichon, Xavier Mininger, Olivier Dubrunfaut, Florian Monsef, Chadi Gannouni, Delong He, Jinbo Bai, Laurent Prevond

Assessment of Broadband Shielding Effectiveness of Composite Panels for Protective Enclosures

Paul Clérico, Lionel Pichon, Xavier Mininger, Olivier Dubrunfaut, Florian Monsef, Chadi Gannouni, Delong He, Jinbo Bai, and Laurent Prévond

***Abstract*—The article investigates the shielding effectiveness (SE) of a metallic enclosure with a multilayer composite cover over a wide frequency range, from near-field magnetic shielding (1 Hz–1 MHz) to far-field electromagnetic shielding (4–14 GHz). Two enclosures are considered: a conductive enclosure made of aluminum and a magnetic enclosure made of steel. The multilayer composite is a trilayer combining a thin conductive layer of graphene and a thin magnetic layer of a Fe-Ni alloy on either side of a fiberglass plate. To determine the SE of these enclosures in both low-frequency and high-frequency approaches, two experimental setups and two numerical models are developed. The use of the composite cover, instead of the metallic one, gives a similar level of SE in the far-field and a higher specific SE (i.e., SE divided by the material density) in the near-field from 1 Hz to 2 kHz. Such quantitative analysis is the first step to designing practical enclosures entirely covered with composite panels to face electromagnetic compatibility (EMC) constraints in embedded systems.**

***Index Terms*—Composite, enclosure, far-field, near-field, shielding effectiveness.**

I. Introduction

In RECENT years, the growing use of electronic devices led to an increase in different sources of disturbance. Electromagnetic interferences (EMI), related to these disturbances, can lead to serious problems in the performance and reliability of electronic systems. Thus, manufacturers design their products to reduce or eliminate the effects of these interferences. The use of electromagnetic shielding as an enclosure is often a solution. Metallic enclosures are commonly used thanks to their natural efficiency to face EMI. In the literature, most studies have focused on the shielding effectiveness (SE) of metallic enclosures, taking into consideration the effects of apertures, wires, or slots [1], [2], [3], [4]. These studies often address frequencies higher than 1 MHz where cavity resonances are observed.

However, to facilitate the integration of embedded devices in the automotive and aircraft industries, lightweight composites present a strong interest. In the framework of increasing electromobility in transportation means, the development of lightweight composite materials will allow the next generation of high-performance economical vehicles. Carbon-based composites are among the most common ones, including carbon nanotubes [5], [6], [7], carbon fibers [8], [9], [10], or graphene [11]. These composites are generally dedicated to high-frequency applications, X-band for example (8–12 GHz) for radar applications. Moreover, metal coatings are sometimes proposed to increase SE [12], [13]. In [14], Multiwalled carbon nanotubes-added glass fabric/epoxy composites used as shielding enclosure show a promising SE, higher than 20 dB between 300 MHz and 1 GHz. In [15], it was observed that the use of a graphene layer coated on the inner surfaces of a rectangular aluminum enclosure can greatly reduce cavity resonances and improves SE between 100 MHz and 2 GHz.

For low-frequency shielding applications, magnetic materials are required. They can provide high SE thanks to their capacity to channel magnetic flux. Multilayer or biphasic composites, that combine both magnetic and conductive metals, show good capabilities [16], [17], [18]. In [19], a permalloy (PC) – aluminum (Al) multilayer was proposed as material for the wall and door of a magnetically shielded room and shows that the Al layer increases the shielding effect of the sandwiched PC-Al-PC combination even for frequencies for which only Al layer has no shielding effect (0.1–10 Hz). In [20], an enclosure constituted of a steel layer and an Al layer separated by an air gap was proposed to reduce the amount of metal employed while improving the shielding performance of magnetic screens at an industrial frequency (50 Hz).

Thus, from the literature, it appears that shielding sheets are either designed for low-frequency applications, from dc to tens of kHz, or for high-frequency applications, from a few MHz to several GHz. Furthermore, most studies on shielding enclosures focused on a restricted frequency range. However, there is a significantly increased range of frequencies in transportation means due to embedded personal communication devices. At the

Manuscript received 29 April 2022; revised 20 July 2022; accepted 6 August 2022. Date of publication 30 August 2022; date of current version 13 October 2022. This work was supported by LabEx LaSIPS (ANR-10-LABX-0032-LaSIPS) and French National Research Agency under the "Investissements d'avenir" program (ANR-11-IDEX-0003). *(Corresponding authors: Paul Clérico; Lionel Pichon.)*

Paul Clérico, Lionel Pichon, Xavier Mininger, Olivier Dubrunfaut, Florian Monsef, and Chadi Gannouni are with the Laboratoire de Génie Electrique et Electronique de Paris, CentraleSupelec, CNRS, Université Paris-Saclay, 91192 Gif-sur-Yvette, France, and also with Sorbonne Université, 75252 Paris, France (e-mail: paul.clerico@centralesupelec.fr; lionel.pichon@centralesupelec.fr; xavier.mininger@centralesupelec.fr; olivier.dubrunfaut@centralesupelec.fr; florian.monsef@centralesupelec.fr; chadi.gannouni@centralesupelec.fr).

Delong He and Jinbo Bai are with the Laboratoire de Mécanique Paris-Saclay, CentraleSupelec, ENS Paris-Saclay, CNRS, Université Paris-Saclay, 91190 Gif-sur-Yvette, France (e-mail: delong.he@centralesupelec.fr; jinbo.bai@centralesupelec.fr).

Laurent Prévond is with the SATIE-CNAM, ENS Paris-Saclay, CNRS, Univeristé Paris-Saclay, 91190 Gif-sur-Yvette, France (e-mail: laurent.prevond@lecnam.net).

Color versions of one or more figures in this article are available at https://doi.org/10.1109/TEMC.2022.3199904.

Digital Object Identifier 10.1109/TEMC.2022.3199904

same time, electrification in transportation means enhances the radiated perturbations of power systems, which mainly operate at low frequency. In this context, there is a strong interest to design and study lightweight composite materials because of providing efficient shielding over a wide frequency range. In [22], the authors proposed a three-layer composite structure combining a thin conductive layer of graphene and a thin magnetic layer of a commercial Fe-Ni alloy, called Mu-ferro [21]. It was previously shown with a modeling approach that the graphene layer allows compensating for the diminution of the SE observed for frequencies higher than 20 kHz due to the decrease of the Mu-ferro permeability. In the case of planar materials, the trilayer composite showed an interesting SE higher than 17 dB for near-field applications, better than an Al or a steel sheet at iso-mass from 1 Hz to 1 kHz. These preliminary numerical results obtained for planar sheets suggested that such composite could provide an adequate solution in 3D realistic configurations.

This current article proposes to assess numerically and experimentally the SE of such a composite in the case of a practical enclosure dedicated to electronic equipment. The novelty of the work is to address a broad-frequency band (from Hz to GHz). As a practical test case, the work analyzes the shielding effectiveness of a metallic enclosure, with a lightweight composite cover. In Section II.A, the dimensions of the enclosure and properties of materials are presented. To study the SE over a wide frequency range including enclosure resonances, two experimental setups, and two 3D numerical models are developed, in Section II.B and Section II.C, respectively. Experimental measurements and numerical results are compared and discussed for low- and high-frequency approaches, in Section III.A and Section III.B, respectively. Finally, some conclusions and perspectives will be drawn in Section IV.

II. Materials, Experimental Setups, and Numerical Models

A. Enclosure and Materials

In this study, two enclosures are considered: a conductive enclosure made of Al and a magnetic enclosure made of steel. The use of the composite cover is compared to the metallic ones. Fig. 1(a) shows a picture of the Al enclosure alongside a schematic transversal cut with the composite cover (Fig. 1(b)). The external sizes of both enclosures are $120 \times 120 \times 92$ mm. The wall thickness is 2 mm. A small square hole (7×7 mm) is made on one side of the enclosure for measurements. Graphene and Mu-ferro layers of the composite are separated by a thick layer of a glass fiber reinforced epoxy composite (GFC), used as mechanical support. Layer thicknesses are 23 μm, 2 mm, and 50 μm for Mu-ferro, GFC, and grapheme, respectively. The high conductive graphene film used in this work is from Prof. Liu's lab at Chalmers University of Technology, Sweden. Details about the production technique and the properties can be found in [23], [24].

The properties of each material are listed in Table I. The conductivity is deduced from resistivity measurements obtained by a four-probe method. Relative permeabilities of steel and

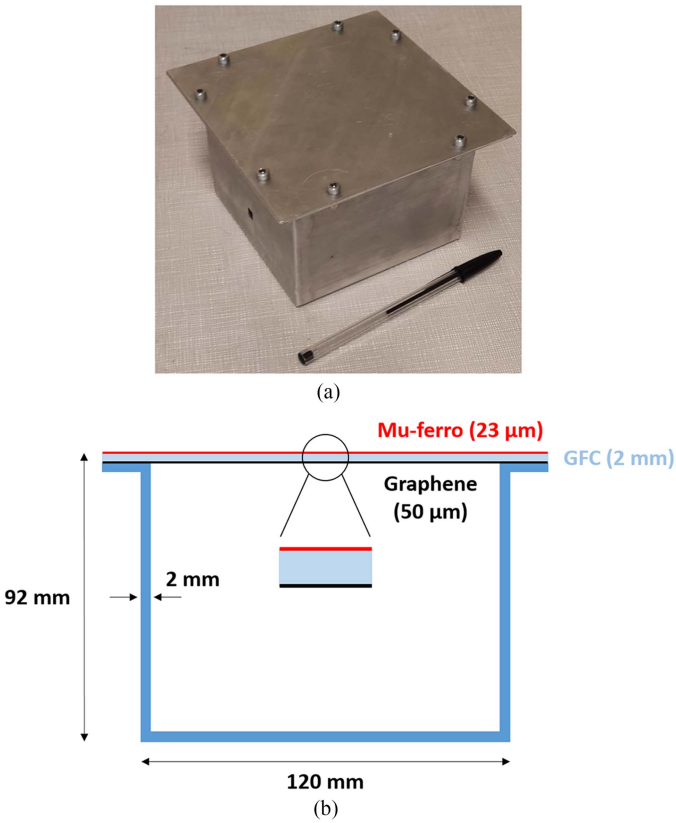

(a)

(b)

Fig. 1. (a) Al enclosure. (b) Schematic diagram with the trilayer composite cover.

TABLE I
Thickness, Conductivity, and Relative Permeability of Each Material

Material	Thickness	Conductivity (S/m)	Relative Permeability
Al	2 mm	35.8e6	1
Steel	2 mm	7.7e6	140 (1 Hz – 1 MHz) 1 (4 GHz – 14 GHz)
Mu-ferro	23 µm	4.8e5	11 380 (1 Hz) 560 (1 MHz) 1 (4 GHz – 14 GHz)
Graphene	50 µm	8.5e5	1
GFC	2 mm	1e-12	1

Mu-ferro are obtained from experimental measurement of the SE of plane sample in the near-field, from 1 Hz to 1 MHz [22]. The relative permeability of steel is considered constant in this frequency range. However, the change in permeability with the frequency of the Mu-ferro layer is taken into account. For far-field (> GHz) simulations, all relative permeabilities are considered equal to 1.

B. Experimental Setups

For the low-frequency range, from 100 Hz to 1 MHz, the shielding effectiveness is determined from the measurements of the magnetic field generated by a coil placed inside the enclosure. An impedance/gain-phase analyzer (HP4104A) is

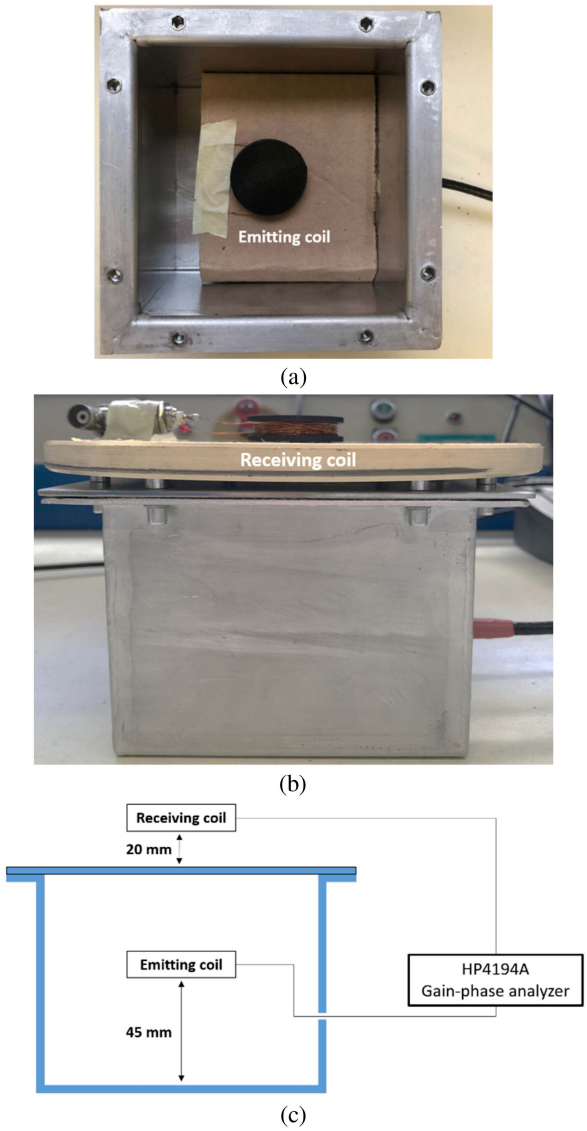

Fig. 2. (a) Experimental setup for the low-frequency shielding measurements, view of the emitting coil centered inside the enclosure. (b) View of the receiving coil above the enclosure. (c) Schematic diagram of the setup.

used to obtain the gain (dB) between two circular coils of 50 turns with a diameter of 3 cm and a height of 1 cm. Fig. 2 shows the experimental setup. The emitting coil is centered inside the enclosure at 45 mm from the bottom [Fig. 2(a)]. The receiving coil is placed above the enclosure at 20 mm [Fig. 2(b)]. The distance between the two coils is then 60 mm.

It was decided for experimental practicality that the reference measurement is the one inside the enclosure without the cover and not, typically, the one in free space. The calculated SE is then more related to the effect of the different covers than to the enclosure itself. This measurement allows obtaining information on the cover and its role in magnetic shielding.

The SE is calculated by

$$\mathrm{SE}_{dB} = \mathrm{Gain}_{wc} - \mathrm{Gain}_{c} \tag{1}$$

where Gain_{wc} is the gain measured without the cover, and Gain_{c} the gain measured with the cover.

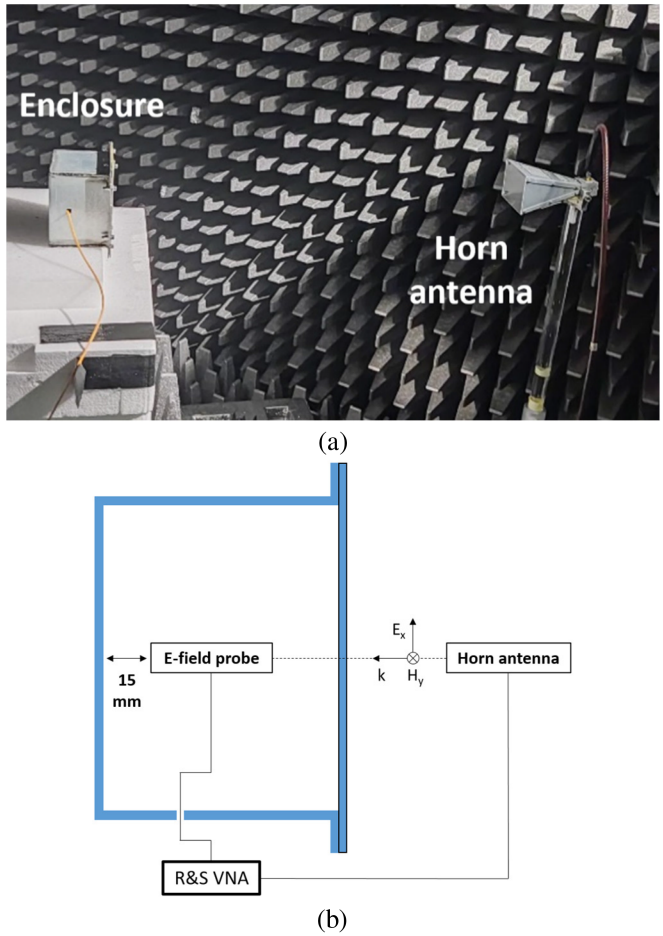

Fig. 3. (a) Experimental setup for the high-frequency shielding measurements, view of the anechoic chamber. (b) Schematic diagram of the setup.

For the high-frequency range, i.e., from 4 to 14 GHz, the SE is determined from the measurement of the electrical field inside the enclosure via an optical probe. A vector network analyzer (R&SZVA67) is used to obtain the transmission coefficient $\mathrm{S21_{dB}}$ between an exciting horn antenna and the optical probe. The measurements are composed of 601 frequencies and are done in an anechoic chamber to avoid disturbances. Fig. 3 shows the experimental setup. A horn antenna (Schwarzbeck BBHA 9120 C), with a frequency range of 2–18 GHz, emits a plane wave polarized following the x-axis and propagating following the z-axis. An E-field probe (Enprobe EFS-105-12), centered inside the enclosure at 15 mm from the bottom, measures the electric field following the x-axis. The distance between the horn antenna and the enclosure is 700 mm.

The SE is calculated in this case by

$$\mathrm{SE}_{dB} = S21_{wc} - S21_{c} \tag{2}$$

where $S21_{wc}$ is the transmission coefficient without the cover and $S21_{c}$ the transmission coefficient with the cover. As in the low-frequency case, for practicality and to obtain information on the cover, the reference measurement is the one without the cover.

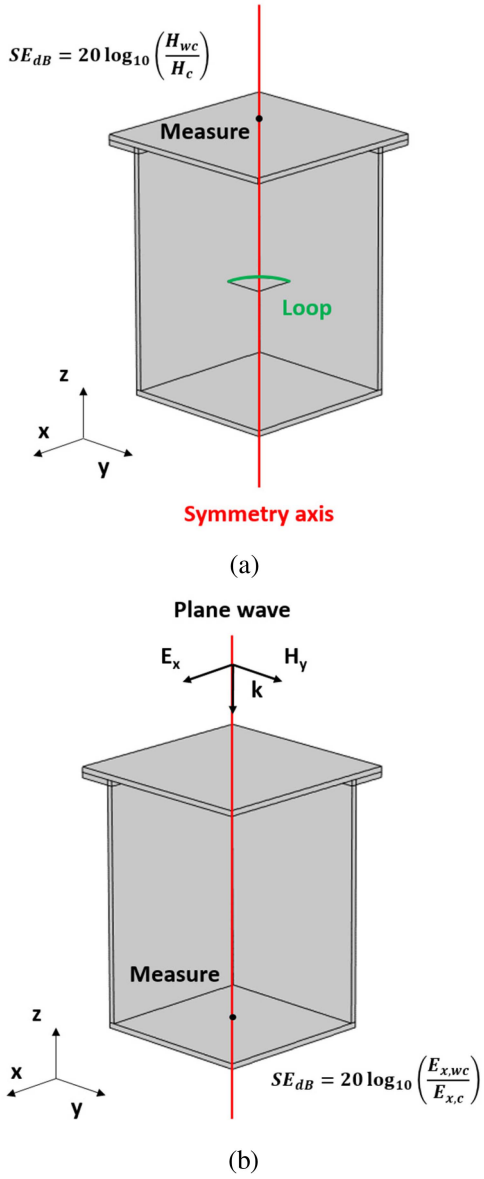

Fig. 4. (a) Geometries of the 3D numerical models for the low-frequency configurations. (b) High-frequency configurations.

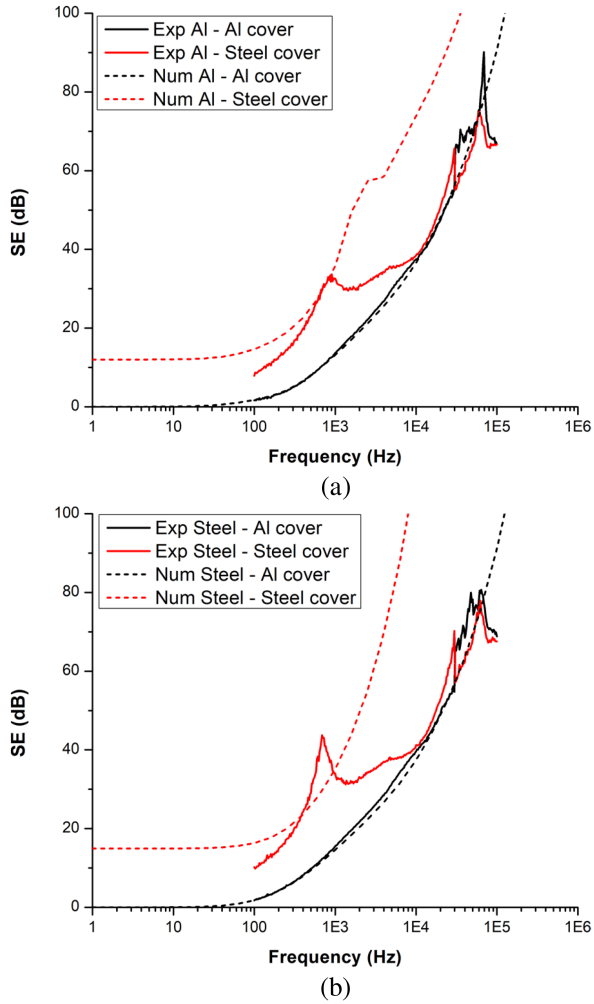

Fig. 5. (a) Experimental and numerical SE of the Al enclosure. (b) Steel enclosure with the Al and steel covers.

C. 3D Numerical Models

Geometries of the two numerical models, corresponding to the experimental setups, are represented in Fig. 4 for the low-frequency (a) and the high-frequency (b) configurations. For both applications, to reduce computation time, only one-quarter of the enclosure is considered.

For the low-frequency configuration, the numerical model is developed with the ac/dc module of COMSOL Multiphysics, a commercial FEM software covering both low-frequency and wave propagation issues. The emitting and receiving coils are respectively simplified by a circular filamentary loop and by a measuring point. For symmetry, the xz and yz planes are defined as magnetic insulation ($n \times A = 0$). A layer of infinite elements bounds the computational domain. Thin-layer modeling is challenging, especially for 3D applications. Thus, a homogenization method [25] and artificial material single layer (AMSL) method [26] are used to simplify numerical calculations. Thanks to the AMSL method, enclosure walls are only meshed by 4-parallelepiped entities in thickness. For the composite cover, the homogenization method is applied before using the AMSL method following [22]. The SE is calculated by computing the magnetic field outside the enclosure, on the symmetry axis, with and without the cover.

For the high-frequency configuration, the numerical model is developed with the radio frequency (RF) module. The E-field probe is reduced to a measuring point. The enclosure is illuminated by a plane wave polarized along the *x*-axis. For symmetry, xz and yz planes are respectively defined as perfect magnetic conductors ($n \times H = 0$) and as perfect electric conductors ($n \times E = 0$). A layer of perfectly matched layers bounds the computational domain. The skin depth is smaller than 100 nm for the studied frequency range (4–14 GHz), it is, therefore, impossible to consider it in the numerical model. Then, only two-tetrahedral entities are considered in the thickness of the walls. The SE is calculated by computing the electric field E_x

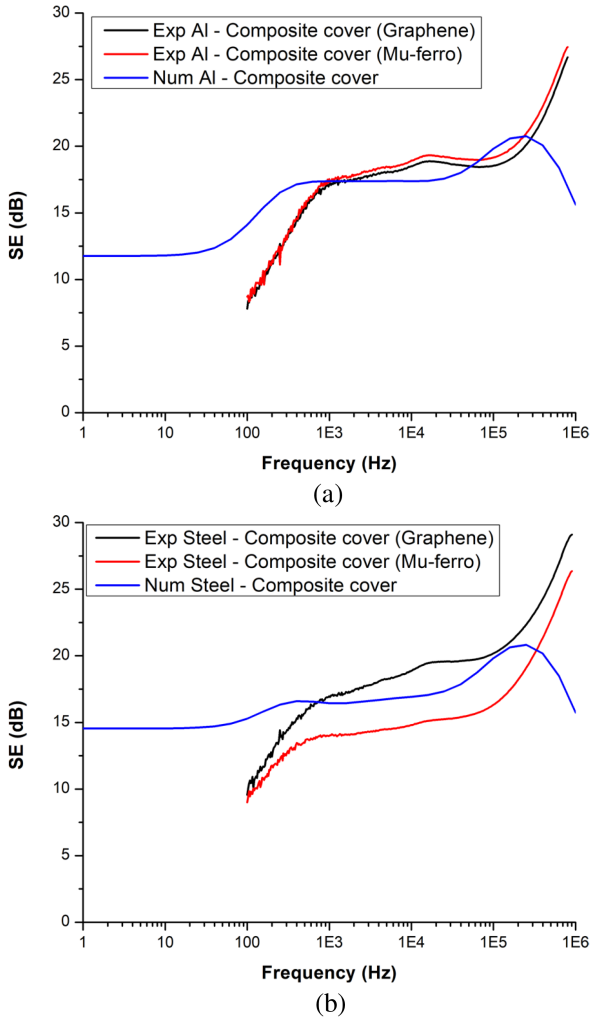

Fig. 6. (a) Experimental and numerical SE of the Al enclosure. (b) Steel enclosure with the trilayer composite cover – The layer in contact with the enclosure is indicated between brackets.

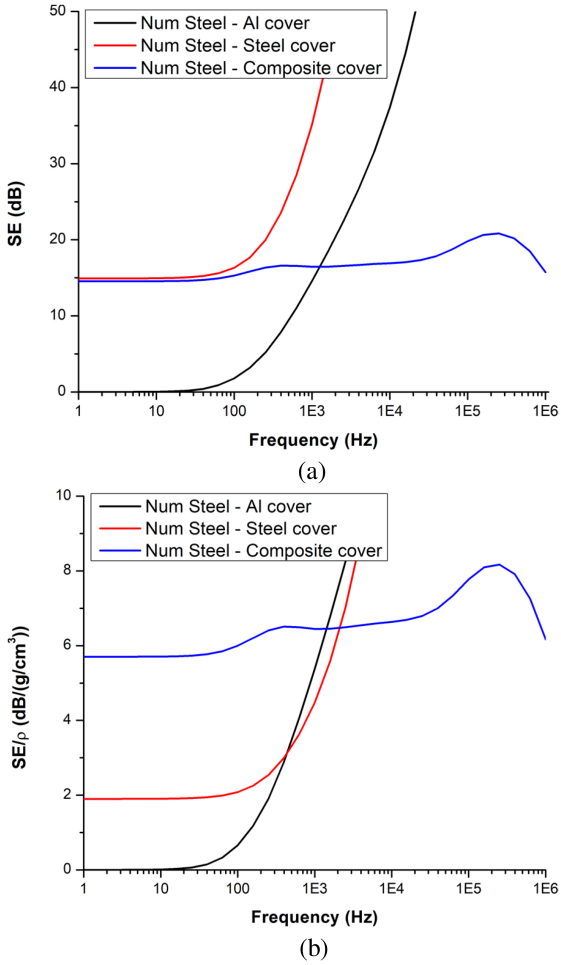

Fig. 7. (a) Numerical SE. (b) Specific SE of the steel enclosure with Al, steel, and composite covers.

inside the enclosure, on the symmetry axis, with and without the cover.

III. Results and Discussion

A. Low-frequency Shielding

Experimental and numerical SE for both Al and steel enclosures are presented in Figs. 5 and 6, with metallic and composite covers, respectively. For both enclosures with the Al cover, the numerical model shows a good agreement with the experimental result from 100 Hz to 30 kHz, before observing some variations in the experimental measurements. However, for the steel cover, the numerical result is significantly higher than the experimental one for the two following reasons detailed in [27]. First, permeability exhibits an imaginary part that is not considered in our simulations and leads to magnetic losses, which are hard to assess in the microwave range. Second, the steel used in our experiments has galvanic protection made of superficial zinc (Zn) layer. Its influence is not included in our simulations as its thickness is not known. As explained in [27], the distribution of the induced currents in the different layers is a function of frequency. From Fig. 5, the distribution may be dominant in the steel layer at very low frequencies (< 1 kHz) and the Zn layer has likely more influence at higher frequencies thus obtaining similar trends with the pure Al case. Furthermore, in the numerical model, a perfect electrical contact between the enclosure and the cover is considered. Experimentally, it is not the case due to the existence of a thin air interstice. This thin interstice may have a greater impact with the steel cover than the Al one.

With the composite cover, experimentally, two configurations can be chosen: either the graphene layer or the Mu-ferro layer is in contact with the enclosure [cf Fig. 1(b)]. The obtained SE with these two orientations is plotted in Fig. 6. With the Al enclosure [Fig. 6(a)], the cover orientation has only a little effect. The SE is slightly higher when the Mu-ferro layer is in contact. On the contrary, with the steel enclosure [Fig. 6(b)], a large difference is observed. The shielding is far more effective when the graphene layer is in contact with the enclosure. A higher conductivity and a better electrical contact between the cover and the enclosure could explain this difference. In the numerical model, the composite cover is homogenized and then

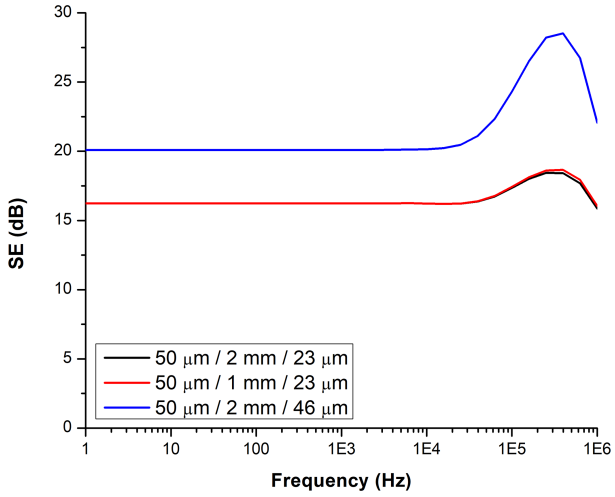

Fig. 8. SE of the trilayer composite (Graphene/GFC/Mu-ferro) obtained with a 2D-axi numerical model presented in [22] for a plane sheet with different thicknesses of the GFC and Mu-ferro layers.

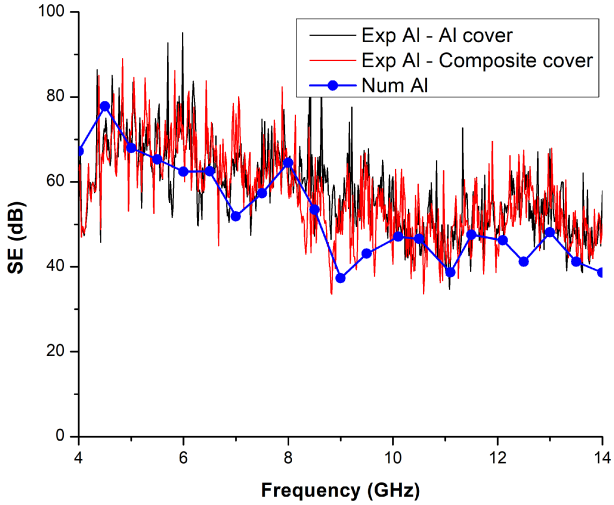

Fig. 9. Experimental and numerical SE of the Al enclosure with the Al and composite covers.

its orientation cannot be considered. However, it is observed that the numerical results are quite close to the experimental ones, from 1 kHz when the latter becomes more valid and less noisy. The diminution of the relative permeability of the Mu-ferro layer with the frequency, considered in the numerical model, is only an approximation and explains the observed decrease of the numerical results after 300 kHz.

In Fig. 7(a), the SE of the steel enclosure with the different covers obtained numerically is plotted on the same graph. Due to their high conductivity, the Al and steel covers present an important increase of the SE with the frequency. Nevertheless, the composite cover gives a better SE from 1 Hz to 1 kHz compared to the Al cover. The obtained SE at low frequencies ($<$ 100 Hz) is similar to the steel cover (15 dB).

However, one of the strengths of the composite is its lightness. Indeed, its density is 2.55 g/cm^3, lower than the ones of Al and steel which are respectively 2.71 and 7.85 g/cm^3. The weight of the different covers is then 107, 114, and 330 g for the composite, Al, and steel covers, respectively. Fig. 7(b) shows the specific SE, i.e., the SE divided by the cover density. In this case, the specific SE of the composite cover is greater than the ones of Al and steel from 1 Hz to around 2 kHz.

It can be noticed that the composite thickness is chosen to have the same thickness as the Al and steel covers. However, the GFC thickness can be reduced without impairing the composite SE as seen in Fig. 8. Moreover, to improve the SE of the composite in the low-frequency range, one possibility is to double the Mu-ferro thickness with a second layer (46 μm instead of 23 μm) without increasing its density too much (2.64 g/cm^3 instead of 2.55 g/cm^3) as presented in Fig. 8. By doubling the thickness of the Mu-ferro, the composite SE increases of 4 dB for frequencies under 10 kHz.

B. High-frequency Shielding

Experimental and numerical SE of the Al enclosure with Al and composite covers are shown in Fig. 9. The SE with the composite cover is nearly identical to the Al one. This is easily understood since, for such a frequency range, the conductivity of the composite is sufficiently high to behave as a perfect conductor. From 4 to 14 GHz, SE tends to decrease from around 70 to 50 dB. The same observation is done with the steel enclosure. The numerical result is quite close to the experimental one and shows the same behavior. Experimental curves present peaks that could be considered as the noise at first glance but corresponds in fact too many cavity resonances (cf Fig. 11). To reduce the computational burden, the frequency response was computed with a frequency step small enough to obtain the global variation of SE, but too large to get all the resonant frequencies of the enclosure. This explains some discrepancies, especially between 9 and 13 GHz. Moreover, it was observed cavity resonances have an important impact on SE in the numerical model. However, it should be emphasized that the SE level obtained with the 3D numerical model has a reasonable agreement with the measurement. Such a magnitude of SE, higher than 50 dB, is promising for many practical electromagnetic compatibility (EMC) applications in embedded systems.

To improve the previous comparison between measurement and numerical predictions, a deeper analysis within some smaller frequency bands was performed. In Fig. 10, experimental and numerical SE of the Al enclosure with the composite cover are plotted between 6–7 GHz and 11–12 GHz. Numerically, new cavity resonances can be identified, respectively, around 6.4 (TE_{303}), 6.95 (TE_{104}), 11.6 (TE_{743}), and 11.75 GHz (TE_{901}). It has been observed, experimentally, that peak positions and magnitudes vary a little from one measurement to another. Numerically, peak magnitudes can also vary from one calculation to another. Thus, the quality of the numerical results around frequencies corresponding to cavity resonances strongly

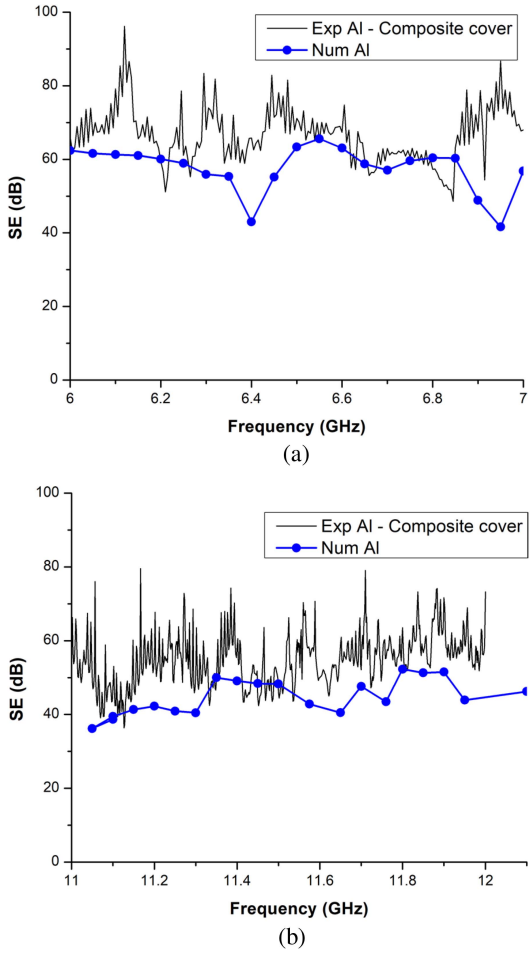

Fig. 10. Experimental and numerical SE of the Al enclosure with the composite cover between 6–7 GHz (a) and 11–12 GHz (b).

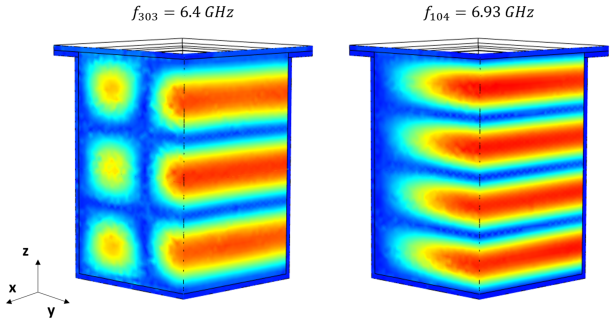

Fig. 11. Electric field E_x distribution inside the enclosure at 6.4 and 6.93 GHz – Observation of cavity resonances.

depends on the frequency step used for the sweep. But, as the main conclusion, this comparison confirms a global reasonable agreement over the range 4–14 GHz.

In Fig. 11, the electric field E_x at resonance frequencies is plotted inside the enclosure. The frequency of cavity resonances can be correctly determined with the numerical model. However, due to boundary conditions to keep symmetry, some resonance frequencies that do not verify these conditions cannot be observed.

IV. Conclusion

In this work, the shielding effectiveness of a three-layer composite as a panel of a 3D enclosure has been determined both numerically and experimentally. In the major conclusion, the proposed composite combines lightness and a high level of SE over a large frequency range, from 1 Hz to 14 GHz. Indeed, its conductivity is high enough to reach a similar SE to Al or steel in the far-field for frequencies from 4 to 14 GHz. In this case, the SE depends mainly on the seam and aperture, as the imperfect contact between the cover and the enclosure is the main path of electromagnetic leakage. Moreover, the high relative permeability of the Mu-ferro layer gives a similar SE (15 dB) to the steel from 1 to 100 Hz. The specific SE (SE divided by the material density) of the composite cover is greater than the Al and steel covers from 1 Hz to 2 kHz. Numerical results are quite close to experimental measurements for both low-frequency and high-frequency approaches and confirms the efficiency of the layered composite.

This article focused only on the enclosure cover, thus in near future, the behavior of an entire enclosure constituted with the trilayer composite will be performed. Also, the mid-range frequency extending from 1 MHz to 4 GHz has not been addressed due to limitations of the experimental setups. It remains to be investigated.

Acknowledgment

The authors would like to thank M. Murugesan from SHT Smart High-Tech AB, Gothenburg, Sweden, and Johan Liu from EMSL, MC2, Chalmers University of Technology, Gothenburg, Sweden, for the supply of the grapheme film.

References

[1] S. Celozzi, R. Araneo, and G. Lovat, "Enclosures," in *Electromagnetic Shielding*. Hoboken, NJ, USA: Wiley, 2008, pp. 164–199, doi: 10.1002/9780470268483.

[2] Q.-F. Liu, W.-Y. Yen, J.-F. Mao, and Z. Chen, "Accurate characterization of shielding effectiveness of metallic enclosures with thin wires and thin slots," *IEEE Trans. Electromagn. Compat.*, vol. 51, no. 2, pp. 293–300, May 2009, doi: 10.1109/TEMC.2008.927942.

[3] H. Azizi, F. T. Belkacem, D. Moussaoui, H. Moulai, A. Bensaoud, and M. Bensetti, "Electromagnetic interference from shielding effectiveness of a rectangular enclosure with apertures – circuit approach, FDTD and FIT modeling," *J. Electromagn. Waves Appl.*, vol. 28, no. 4, pp. 494–514, 2014, doi: 10.1080/09205071.2013.875862.

[4] A. Shouvarzi and M. Joodaki, "Shielding effectiveness estimation of a metallic enclosure with an aperture using S-parameter analysis: Analytic validation and experiment," *IEEE Trans. Electromagn. Compat.*, vol. 59, no. 2, pp. 537–540, Apr. 2017, doi: 10.1109/TEMC.2016.2615525.

[5] Y. Liu et al., "Go-CNTs hybrids reinforced epoxy composites with porous structure as microwave absorbers," *Composites Sci. Technol.*, vol. 200, 2020, Art. no. 108450, doi: 10.1016/j.compscitech.2020.108450.

[6] X. Fan et al., "Study on foamability and electromagnetic interference shielding effectiveness of supercritical CO_2 foaming epoxy/rubber/MWCNTs composite," *Composites Part A: Appl. Sci. Manuf.*, vol. 121, pp. 64–73, 2019, doi: 10.1016/j.compositesa.2019.03.008.

[7] Y. Xie et al., "Microwave-assisted foaming and sintering to prepare lightweight high-strength polystyrene/carbon nanotube composite foams with an ultralow percolation threshold," *J. Mater. Chem.*, vol. 9, pp. 9702–9711, 2021, doi: 10.1039/D1TC01923F.

[8] D. D. L. Chung and A. A. Eddib, "Effect of fiber lay-up configuration on the electromagnetic interference shielding effectiveness of continuous carbon fiber polymer-matrix composite," *Carbon*, vol. 141, pp. 685–691, 2019, doi: 10.1016/j.carbon.2018.09.081.

[9] A. Ameli, P. U. Jung, and C. B. Park, "Electrical properties and electromagnetic interferences shielding effectiveness of polypropylene /carbon fiber composites foams," *Carbon*, vol. 60, pp. 379–391, 2013, doi: 10.106/j.carbon.2013.04.050.

[10] W. Abdelli, X. Mininger, L. Pichon, and H. Trabelsi, "Impact of composite materials on the shielding effectiveness of enclosures," *Appl. Comput. Electromagn. Soc. J.*, vol. 27, no. 4, pp. 369–374, 2012.

[11] W. L. Song et al., "Flexible graphene/polymer composite films in sandwich structures for effective electromagnetic interference shielding," *Carbon*, vol. 66, pp. 67–76, 2014, doi: 10.1016/j.carbon.2013.08.043.

[12] J. Lee, B. M. Jung, S. B. Lee, S.-K. Lee, and K. H. Kim, "FeCoNi-coated glass fabric/polycarbonate composite sheets for electromagnetic absorption and shielding," *IEEE Trans. Magn.*, vol. 53, no. 11, pp. 1–4, Nov. 2017, doi: 10.1109/TNAG.2017.2704663.

[13] Y. Liu, D. He, O. Dubrunfaut, A. Zhang, L. Pichon, and J. Bai, "Hybrids of glass fibers coated with carbon nanotubes and nickel for high-performance electromagnetic wave absorption composites," *J. Appl. Polym. Sci.*, vol. 139, no. 9, 2022, Art. no. 51727, doi: 10.1002/app.51727.

[14] K.-Y. Park, S.-E. Lee, C.-G. Kim, and J.-H. Han, "Application of MWCNT-added glass fabric/epoxy composites to electromagnetic wave shielding enclosures," *Composite Structures*, vol. 81, no. 3, pp. 401–406, 2007, doi: 10.1016/j.compstruct.2006.08.029.

[15] S. Güler and S. Yenikaya, "Analysing the shielding effectiveness of graphene sheet coated rectangular enclosure," *Electromagnetics*, vol. 41, no. 7, pp. 469–475, 2021, doi: 10.1080/02726343.2021.2012938.

[16] P. Clérico, X. Mininger, L. Prévond, T. Baudin, and A.-L. Helbert, "Magnetic shielding of a thin Al/steel/Al composite," *COMPEL*, vol. 39, pp. 595–609, 2020, doi: 10.1108/COMPEL-09-2019-0374.

[17] X. Ma, Q. Zhang, Z. Luo, X. Lin, and G. Wu, "A novel structure of Ferro/Aluminum based sandwich composite for magnetic and electromagnetic interference shielding," *Mater. Des.*, vol. 89, pp. 71–77, 2016, doi: 10.1016/j.matdes.2015.09.137.

[18] A. O. Watanabe, P. M. Raj, D. Wong, R. Mallapudi, and R. Tummala, "Multilayered electromagnetic interference shielding structures for suppressing magnetic field coupling," *J. Electron. Mater.*, vol. 47, pp. 5243–5250, 2018, doi: 10.1007/s11664-018-6387-2.

[19] K. Yamazaki, K. Kato, and K. Fujiwara, "Effective combination of magnetic and conductive layers of magnetically shielded room [for biomagnetic measurements]," *IEEE Trans. Magn.*, vol. 36, no. 5, pp. 3649–3651, Sep. 2000, doi: 10.1109/20.908929.

[20] O. Losito, F. Rella, V. Dimiccoli, F. Pagliaria, and B. Audone, "Shielding improvement of multilayer enclosure at low frequency," in *Proc. Int. Symp. Electromagn. Compat.*, 2013, pp. 1004–1007.

[21] Holland Shielding Systems BV. 2021. Accessed: Jun. 1, 2021. [Online]. Available: https://hollandshielding.com/Mu-ferro-tape-foil

[22] P. Clérico et al., "Design of a lightweight multilayered composite for DC to 20 GHz electromagnetic shielding," *Electronics*, vol. 10, no. 24, 2021, Art. no. 3144, doi: 10.3390/electronics10243144.

[23] N. Wang et al., "Tailoring the thermal and mechanical properties of graphene film by structural engineering," *Small*, vol. 14, no. 29, 2018, Art. no. 18011346, doi: 10.1002/smll.201801346.

[24] S. Guo, J. Chen, Y. Zhang, and J. Liu, "Graphene-based films: Fabrication, interfacial modification, and applications," *Nanomaterials*, vol. 11, no. 10, 2021, Art. no. 2539, doi: 10.3390/nano11102539.

[25] P. Clérico, X. Mininger, L. Prévond, T. Baudin, and A.-L. Helbert, "Compromise between magnetic shielding and mechanical strength of thin Al/steel/Al sandwiches produced by cold roll bonding: Experimental and numerical approaches," *J. Alloys Compounds*, vol. 798, pp. 67–81, 2019, doi: 10.1016/j.jallcom.2019.05.243.

[26] S. Cruciani, T. Campi, F. Maradei, and M. Feliziani, "Conductive layer modeling by improved second-order artificial material single-layer method," *IEEE Trans. Antennas Propag.*, vol. 66, no. 10, pp. 5646–5650, Oct. 2018, doi: 10.1109/TAP.2018.2854413.

[27] A. Cozza and F. Monsef, "Power dissipation in reverberation chamber metallic surfaces based on ferrous materials," *IEEE Trans. Electromagn. Compat.*, vol. 61, no. 6, pp. 1714–1725, Dec. 2019, doi: 10.1109/TEMC.2018.2873657.